Geophysical Research Letters

RESEARCH LETTER
10.1029/2024GL108369

Record High Sea Surface Temperatures in 2023

Boyin Huang[1], Xungang Yin[1], James A. Carton[2], Ligang Chen[2], Garrett Graham[3], Patrick Hogan[1], Thomas Smith[4], and Huai-Min Zhang[1]

[1]NOAA/NCEI, Asheville, NC, USA, [2]Department Atmos. Oceanic Science, University Maryland, College Park, MD, USA, [3]North Carolina Institute for Climate Studies, North Carolina State University, Asheville, NC, USA, [4]NOAA/Center for Satellite Applications and Research, College Park, MD, USA

Key Points:

- Global mean sea surface temperature (SST) in 2023 set a record high
- Record-high SST was associated with widespread marine heatwaves (MHWs) and super-MHWs throughout the oceans
- Record-high SST was attributed to the multi-decadal warming trend, warm phase of Pacific-Atlantic-Arctic mode, and 2023–24 El Niño event

Supporting Information:

Supporting Information may be found in the online version of this article.

Correspondence to:

B. Huang and X. Yin,
boyin.huang@noaa.gov;
xungang.yin@noaa.gov

Citation:

Huang, B., Yin, X., Carton, J. A., Chen, L., Graham, G., Hogan, P., et al. (2024). Record high sea surface temperatures in 2023. *Geophysical Research Letters*, *51*, e2024GL108369. https://doi.org/10.1029/2024GL108369

Received 16 JAN 2024
Accepted 9 JUL 2024

Author Contributions:

Conceptualization: Boyin Huang
Investigation: Boyin Huang, Xungang Yin, James A. Carton
Methodology: Boyin Huang, Xungang Yin
Project administration: Huai-Min Zhang
Software: Boyin Huang, Xungang Yin
Supervision: Patrick Hogan, Huai-Min Zhang
Validation: Xungang Yin, James A. Carton
Visualization: Boyin Huang, Xungang Yin
Writing – original draft: Boyin Huang, Xungang Yin

© 2024 The Author(s). This article has been contributed to by U.S. Government employees and their work is in the public domain in the USA.
This is an open access article under the terms of the Creative Commons Attribution License, which permits use, distribution and reproduction in any medium, provided the original work is properly cited.

Abstract NOAA Daily Optimum Interpolation Sea Surface Temperature (DOISST) and other similar sea surface temperature (SST) products indicate that the globally averaged SST set a new daily record in March 2023. The record-high SST in March was immediately broken in April, and new daily records were set again in July and August 2023. The SST anomaly (SSTA) persisted at a record high from mid-March to the remainder of 2023. Our analysis indicates that the record-high SSTs, and associated marine heatwaves (MHWs) and even super-MHWs, are attributed to three factors: (a) a long-term warming trend, (b) a shift to the warm phase of the multi-decadal Pacific-Atlantic-Arctic (PAA) mode, and (c) the transition from the triple-dip succession of La Niña events to the 2023–24 El Niño event.

Plain Language Summary Observation-based analyses such as the NOAA DOISST show that global mean SST reached a record high in April 2023, breaking the previous record of global mean SST set in March 2016, and the April 2023 record of global mean SST was broken again in July and August 2023. Our study indicates that these record-breaking SSTs in 2023 resulted from record-high SSTs over much of the global oceans and associated with widespread marine heatwaves (MHWs). Further analyses show that the record-high SSTs are attributed to a long-term-warming trend associated with increasing greenhouse gases, a shift to the warm phase of a multidecadal Pacific-Atlantic-Arctic (PAA) mode, and a warming associated with the transition from 2020–23 La Niña events to the 2023–24 El Niño event.

1. Introduction

The globally (90°S–90°N) averaged SST estimated from NOAA Daily Optimum Interpolation Sea Surface Temperature (DOISST) version 2.1 (v2.1; Huang, Liu, et al., 2021) reached 18.83°C on 4 April 2023 (Figure 1a). This may have broken the previous record set on 6 March 2016 (18.78°C), which occurred during the historically strong 2015–16 El Niño event (Huang et al., 2016; L'Heureux et al., 2017). An unusual feature of this record-breaking SST is that it happened immediately after a succession of triple-dip 2020–23 La Niña events (Li et al., 2023), during which the tropical Pacific SSTs were anomalously low. In contrast, record-high SSTs usually occur during or soon after El Niño events, such as in 27 August 2015 (18.66°C), and 6 March 2016 (18.78°C; Figure 1a). The globally averaged SST continued to increase during July and August 2023, and new daily records were set repeatedly as the 2023–24 El Niño event intensified. This record-breaking SST in August 2023 is also seen in other SST products (Brasnett & Colan, 2016; Donlon et al., 2012; Rayner et al., 2003), although their SST values were slightly different (Figure S1 in Supporting Information S1). Although the globally averaged SST decreased after August 2023 following its normal seasonal cycle, the SST anomaly with respect to the 1982–2011 climatology remained record high throughout 2023. These record-breaking SSTs were manifested by extremely strong marine heatwaves (MHWs; Amaya et al., 2023; Huang, Wang, et al., 2021; Holbrook et al., 2019; Oliver et al., 2018; Sen Gupta et al., 2020). The purposes of this study are to review the evolution of the record-breaking SSTs in 2023 and discuss the contributing factors.

2. Data Sets and Methods

2.1. Data Sets

The DOISST v2.1 is a global daily SST product with a resolution of 0.25° × 0.25° starting from September 1981 (Huang, Liu, et al., 2021), which blends in situ SSTs from ships, buoys, Argo floats, and satellite SSTs. The satellite SSTs are from the Advanced Very High-Resolution Radiometer (AVHRR) SST measurements and

Writing – review & editing:
Boyin Huang, Xungang Yin, James A. Carton, Ligang Chen, Garrett Graham, Patrick Hogan, Thomas Smith, Huai-Min Zhang

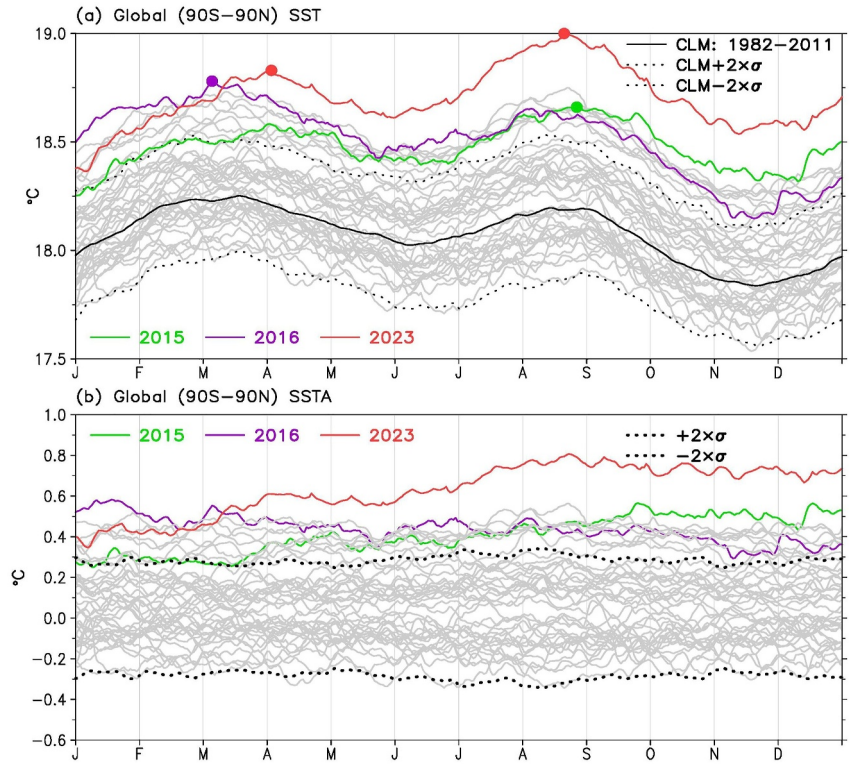

Figure 1. Globally (90°S–90°N) averaged (a) sea surface temperature (SST) and (b) SSTA from 1982 to 2023 represented by gray lines except for 2015, 2016, and 2023. The new SST records were noted with solid circles on 27 August 2015, 6 March 2016, 4 April 2023, and 21 August 2023. The climatology (CLM) and its two standard deviation (2σ) intervals are noted.

Advanced Clear-Sky Processor for Ocean (ACSPO; Ignatov et al., 2016) SSTs. The satellite SST biases are adjusted according to in situ observations (Huang et al., 2017a; Huang, Liu, et al., 2021).

The Extended Reconstructed SST version 5 (ERSSTv5) is a long-term (starting from 1854) monthly 2° × 2° SST product derived from in situ observations from ships, buoys, and Argo floats.

The UK Met Office Operational Sea Surface Temperature and Ice Analysis (OSTIA) v2 is a daily 0.05° × 0.05° SST product starting from 1985 (Donlon et al., 2012). OSTIA includes in situ SSTs from ships and buoys, and a variety of satellite instruments.

The Canadian Meteorological Center SST (CMC; Brasnett & Colan, 2016) v3 is a daily 0.1° × 0.1° SST starting from September 1991. CMC v3 uses in situ SSTs from ships and drifting buoys, and a variety of satellite instruments.

The UK Hadley Center Ice and SST (HadISST; Rayner et al., 2003) is a long-term (starting from 1870) monthly 1° × 1° product derived from in situ ships, buoys, and satellite AVHRR observations after the 1980s.

Ice concentration data are from HadISST version 2 (HadISST2; 1970–2015; Titchner & Rayner, 2014) in monthly 1° × 1° resolutions and NCEP (in and after 2016; Grumbine, 2014) in daily 0.25° × 0.25° resolutions.

Surface air temperature (SAT) data are from the fifth generation European Centre for Medium-Range Weather Forecasts (ECMWF) Reanalysis (ERA5; 1950–2020; Hersbach et al., 2020) in monthly 0.25° × 0.25° resolutions.

2.2. Methods

Using DOISST, the warm SST is characterized by MHWs, which are defined by commonly used criteria that (a) SSTAs are higher than the 90th percentile threshold based over the 1982–2011 period, and (b) the high SSTAs are sustained for at least five consecutive days with gaps of less than 3 days (Amaya et al., 2023; Hobday et al., 2016; Holbrook et al., 2019; Huang, Wang, et al., 2021; Sen Gupta et al., 2020). To describe the extremeness of the SSTs

over the region of MHWs in 2023, super-MHWs are defined when the daily SST in 2023 exceeds the corresponding maximum daily SST (SSTx) from the period of 1982–2022.

To understand the reasons for the record-high SSTs in 2023, the linear trends of SSTAs from monthly ERSSTv5 are calculated and filtered out. The detrended SSTAs are then decomposed into their first two Empirical Orthogonal Functions (EOF1 and EOF2) (Kutzbach, 1967). EOF1 is associated with the El Niño and Southern Oscillation (ENSO) modes at timescale of 3–7 yrs (Philander, 1989). EOF2 is identified as a low-frequency mode in the North Pacific, the North Atlantic, and the Arctic Oceans north of 30°N at timescale of approximately 70 yrs, which is defined as the Pacific-Atlantic-Arctic (PAA) mode in this study.

3. Results

3.1. Record High SSTs

As shown in Figure 1a, the globally averaged SST in DOISST may have reached a record high since 1982 on 4 April 2023 (18.83°C). This record was broken again in mid-July and reached a new record high on 21 August (19.00°C). After removing the climatological daily SST (computed over 1982–2011) at each spatial location, we see that the globally averaged daily SSTA (0.81°C; Figure 1b) on the latter date is about 5 times the standard deviation ($\sigma = 0.16$°C), which exceeds the expected daily climatological value at the 99% significance level. The record-high SSTA persisted from mid-March to the end of 2023.

These record-high globally averaged SSTs in 2023 result from the record-high SSTs in some regions of global oceans (Figure S2 in Supporting Information S1): The SSTs were record high in the North Pacific, North Atlantic and Southern Oceans in or after March 2023, and were near record high in the tropical Pacific and Indian Ocean after August 2023.

In August 2023, for example, the average SSTAs were high in the tropical Pacific (1°−3°C), the North Pacific north of 30°N (2°−6°C), the North Atlantic (2°−5°C), the Arctic coastal zone (2°−6°C), the tropical Indian Ocean (1°C), and the Southern Ocean (1°−2°C) (Figure 2a). These high SSTAs are manifested strong MHWs (Figure 2b), defined by the criterion of SSTAs higher than the 90th percentile over 1982–2011. The MHW intensity in the cumulative SSTAs in units of degree-day (DD) is clearly seen in the tropical Pacific (20−100 DD), the North Pacific north of 30°N (20−150 DD), the North Atlantic (20−100 DD), the Arctic coastal zone (>150 DD), the tropical Indian Ocean west of 90ºE (20 DD), and the Southern Ocean (20−50 DD).

Those high SSTAs in Figure 2a can further be characterized by the super-MHWs (SST-SSTx; Figure 2c) where SSTs break the historic year-day record since 1982. Figure 2c clearly shows such super-MHWs occurring in the central tropical Pacific near the dateline (0.1°−0.2°C), the eastern tropical Pacific east of 120°W (0.1°−0.5°C), the North Pacific north of 30ºN (0.2°−1.0°C), the northern tropical Atlantic between the equator and 30ºN (0.2°−0.5°C), the northwestern North Atlantic south of Greenland (0.5°C), the Arctic coastal zone (0.5°−2.0°), the western Indian Ocean west of 90ºE (0.2°−1.0°C), and the Southern Ocean (0.2°−1.0°C). These geographic patterns of the super-MHWs are very consistent with the maximum SSTAs of MHWs reported in Sen Gupta et al. (2020).

3.2. Reasons for the Record-High SST

The question is: what caused the record-high SSTs in August 2023? We address this question by examining a decomposition of SSTA into three components: a warming trend, EOF1 representing the El Niño and Southern Oscillation (ENSO), and EOF2 representing the PAA mode.

Using ERSSTv5, the SST warming trends over 1950–2023 were calculated (Figure 3a), which show overall SST warming over almost the entire global oceans. In particular, the SST trends are high in the tropical Indian Ocean and western Pacific (0.10°−0.15°C per decade; °C/dec), the western-central South Pacific over 30°S–50°S (0.10°−0.15°C/dec), the Bering Sea (0.25°C/dec), the northwestern North Atlantic (0.25°C/dec), the tropical Atlantic (0.10°−0.20°C/dec), the western South Atlantic (0.25ºC/dec), and the Arctic coastal zone (0.25°C/dec). The pattern of these SST trends is, to some degree, similar to that of SSTAs shown in Figure 2a. For example, both SSTAs and SST trends were high in the North Atlantic, particularly the northwestern North Atlantic. To explore the contribution of this persistent SST warming trend to the record-high SSTs of 2023, the trend of SSTs computed at each location was removed and the detrended SSTA was computed. The globally averaged SSTAs

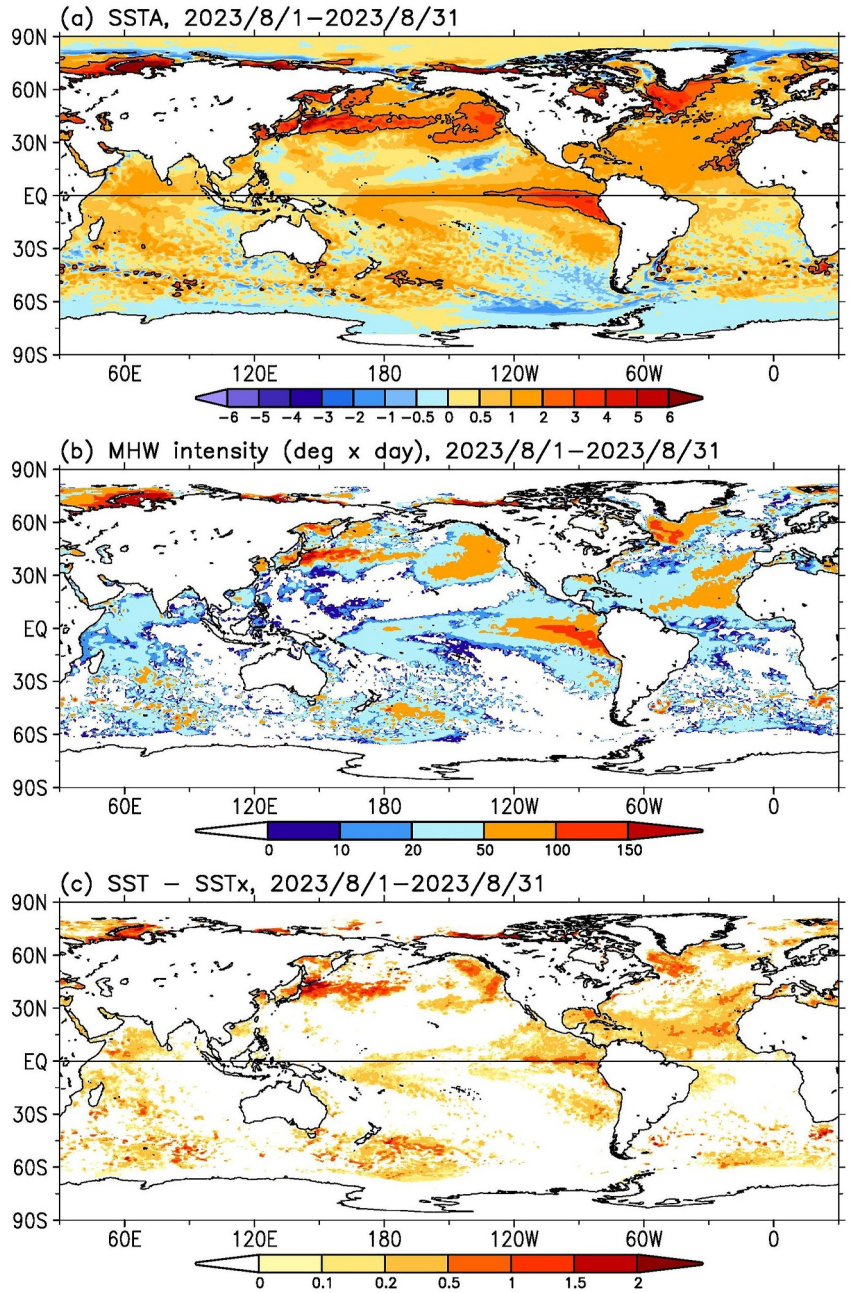

Figure 2. Record-high SSTAs in August 2023 expressed in (a) average SSTAs (°C), (b) conventional MHW intensity index (degree-day), and (c) super-MHW intensity (°C).

with and without trends are compared in Figure 3b. This comparison shows that the high SSTAs since the 2010s were largely a result of this long-term warming trend. In August 2023 the global average SSTA decreased from +0.7°C to +0.4°C after this detrending.

The detrended global SSTAs were then decomposed into EOF1, EOF2, and their associated principal components PC1 and PC2. EOF1 (Figure 3c) represents a typical ENSO pattern, whose magnitude fluctuates between 3 and 7 yrs (Philander, 1989) seen in PC1 (Figure 3d). EOF1 explains 17% of the detrended SSTA variance, with large contributions from the central-eastern tropical Pacific, eastern North Pacific, the central South Pacific south of 40°S, and the western tropical Indian Ocean. Indeed, the globally averaged SSTA after detrending is clearly associated with ENSO evolution represented by PC1 or commonly the Niño3.4 index (Zebiak & Cane, 1987). The

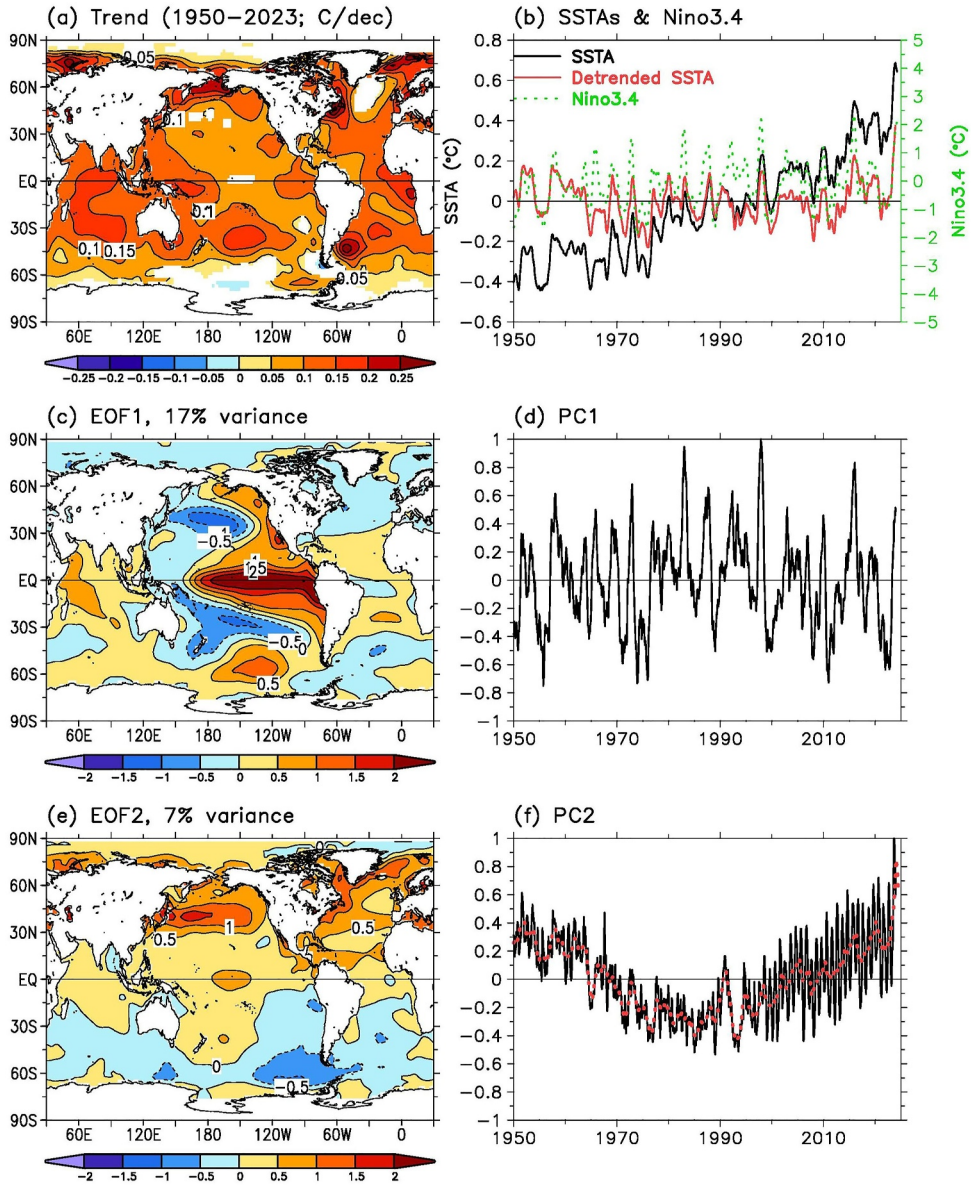

Figure 3. (a) SSTA trends (°C per decade) over 1950–2023, (b) Globally averaged SSTA, detrended SSTA, and Niño3.4 index, (c) EOF1, (d) PC1, (e) EOF2, and (f) PC2 of the detrended monthly SSTA. Trends with significance level lower than 95% have been masked out in (a). A dotted-line with a 12-month filter is overlapped in (f).

correlation coefficient between the detrended SSTA and Niño3.4 index (Figure 3b) is 0.6, which is significant at the 99% level.

The largest loading of the PAA mode, which is represented by EOF2, is found in the North Pacific north of 30°N, the North Atlantic north of 20°N, and the Arctic coastal zone (Figure 3e), which explains 6% of the detrended SSTA variance over the global oceans. The explained variance increases to 12% when the analysis is confined within the Northern Hemisphere oceans. As shown in Figure 3f, the PAA spans about 70 yrs, and it was in its warm phase in the 1950–60s, cold phase in the 1970–90s, and warm phase again in the 2010–20s. The spatial distribution of PAA north of 30°N is very similar to the patterns of the high SSTAs observed in August 2023 in Figure 2a, and the warm phase of PAA after the 2010s matches the strong warming in 2023. This distribution and coincidence with high SSTs suggest a close relationship between PAA and the record-high SSTs in 2023. The sensitivity of the PAA mode to data periods and data sets will be discussed in Section 4.

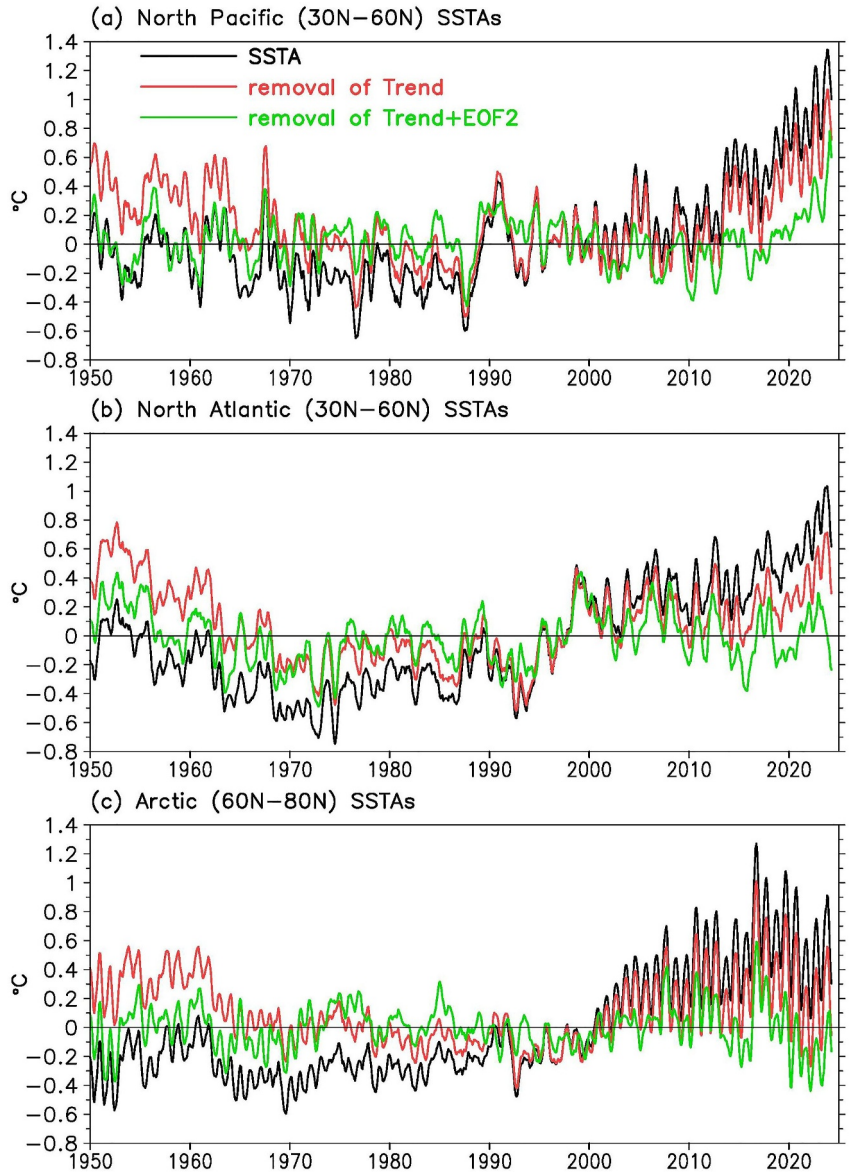

Figure 4. Averaged SSTA (°C), and SSTAs after removal of Trend and Trend + EOF2 in the (a) North Pacific (30°N–60°N), (b) North Atlantic (30°N–60°N), and (c) Arctic (60°N–80°N).

The connection between the phase of the PAA and the record-high SSTAs in the PAA regions is shown by the area-weighted average SSTAs in the North Pacific north of 30°N (Figure 4a), the North Atlantic over 30°N–60°N (Figure 4b), and the Arctic coastal zone over 60°N–80°N (Figure 4c). When the SST trends were subtracted out, the averaged SSTAs are greatly reduced in the North Pacific after the 2010s and in the North Atlantic and the Arctic coastal zone after the 2000s. These SSTAs are further reduced when the PAA mode is removed by subtracting the multiplication of EOF2(x, y) and PC2(t). On average (1950–2023), the SSTA variances over 30°N–80°N decrease by 31%–44%, 25%–42%, and 1%–3%, respectively, due to detrending and removing PAA and ENSO projections (Table S1 in Supporting Information S1). In contrast, the variances in the global oceans over 90°S–90°N decrease by 84%, 5%, and 5%, respectively, indicating the dominant role of the warming trend in global SST change.

We note that clear seasonal fluctuations can be seen in PC2 (Figure 3f) and the Arctic SSTAs (Figure 4c) after about 1995, which peak in the boreal summer (July–September) and plunge in boreal winter (January–March). This suggests that the role of PAA in the SSTs in the PAA region is particularly strong during boreal summer,

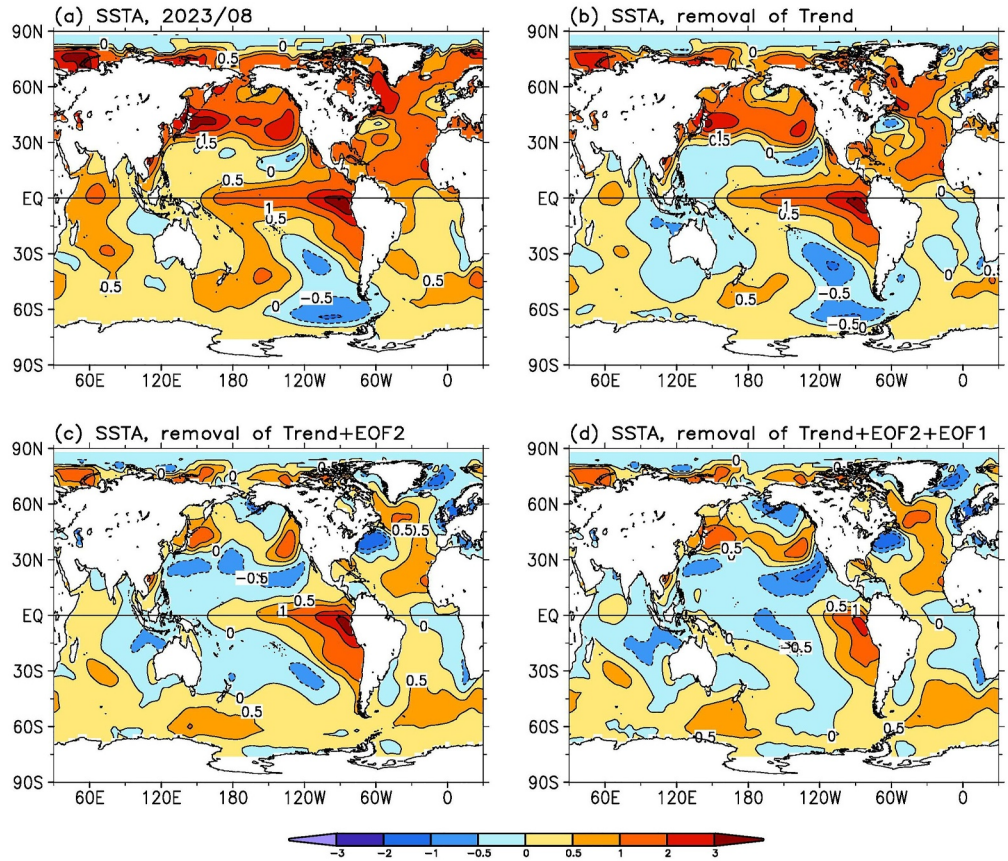

Figure 5. SSTA (°C) in August 2023 (a), and SSTAs after removal of (b) Trend, (c) Trend + EOF2, and (d) Trend + EOF2 + EOF1.

while its role is relatively weak during boreal winter. The seasonal fluctuations of PAA may result from melted sea-ice in high-latitude (https://climate.metoffice.cloud/sea_ice.html; Huang et al., 2017a) and therefore higher SSTs in summer while SST is at a constant freezing point in winter. The reduction in sea-ice area is much faster in boreal summer (Figure S3 in Supporting Information S1) than in winter.

The monthly SSTAs in August 2023 are displayed in Figure 5 when (a) the warming trend, (b) the PAA mode [EOF2(x, y) × PC2(t)], and (c) the ENSO mode [EOF1(x, y) × PC1(t)] are successively subtracted. The original SSTAs (Figure 5a) are high in central-eastern tropical Pacific (1°−3°C), the North Pacific (2°−3°C) north of 30°N, the North Atlantic (1°−2°C), the Arctic coastal zone (1°−3°C), the western Indian Ocean (1°C), and the South Pacific east of New Zealand (1°C). After removing the warming trends (Figure 5b), these SSTAs are reduced by about 0.5°C in those regions except for the tropical Pacific where warming trends are small as shown in Figure 3a. After further removing the PAA mode (Figure 5c), SSTs are further reduced by about 0.5°−1.0°C in the North Pacific north of 30°N, the North Atlantic, and the Arctic coastal zone. When the ENSO mode is removed (Figure 5d), the SSTAs in the central-eastern tropical Pacific are reduced by 0.5°−1.0°C, but part of the SSTA remains in the east due to the existence of ENSO influence not represented by the first ENSO mode. The globally averaged SSTA variances are 0.59, 0.48, 0.34, and 0.29 K^2 in Figures 5a–5d, respectively, indicating clear contributions of the warming trends (19%), PAA (24%), and ENSO (8%) to the record-high SSTs in August 2023. The impact of the detrending and the effects of PAA and ENSO modes on SST changes is demonstrated in Figures S4 and S5 of Supporting Information S1.

4. Summary, Discussion, and Conclusion

The SST analyses based on NOAA DOISST show that globally (90°S–90°N) averaged daily SSTs appeared at record high since 1982 on 4 April 2023 (18.83°C), and that record was continually broken from 16 July until 21

August 2023 (19.00°C). These record-high SSTs resulted from record-high SSTs in the tropical Pacific, the North Pacific north of 30°N, the North Atlantic, the Arctic coastal zone, the tropical Indian Ocean, and the Southern Ocean. The record-high SSTs were manifested by strong MHWs and even super-MHWs. Our analyses indicate that the record-high SSTs in the summer of 2023 were the result of the superposition of three contributors: the long-term warming trend associated with increasing greenhouse gases (Schmidt et al., 2014); the warm phase of the broad multidecadal PAA mode after the 2010s which is most pronounced in the boreal summer; and finally, the increasing temperature associated with the transition from the cool La Niña (2020–23) to the warm El Niño conditions beginning in 2023. Without the long-term warming trend, the other factors would have produced a relatively warm year. It was the combination of all factors that produced the record warmth. It should be noted that there may be other contributors to fully explain the residual SSTAs shown in Figures 4 and 5d. As reported by Kuhlbrodt et al. (2024) and Schmidt (2024), full physical mechanisms for the extreme SSTs in 2023 need further exploring.

The daily global records set by DOISST in 2015 and 2023 generally correspond to records set in other SST data sets including OSTIA and CMC (Figure S1 in Supporting Information S1) but not always. For example, the DOISST record high on 4 April 2023 was not found in OSTIA and CMC. Such differences mainly result from the use of different algorithms for ship-SST bias correction, satellite-SST bias correction, and different spatial resolutions in analyses (Huang et al., 2023), which may represent the structural uncertainty of data analysis (Parker, 2013; Yang et al., 2021). The uncorrected residual bias of −0.04° to −0.05°C in DOISST (Huang et al., 2023) may also suggest the record-high SST on 4 April 2023 (18.83°C) may not be significantly different compared to the previous record on 6 March 2016 (18.78°C).

The warming trends and EOFs were analyzed using monthly ERSSTv5 from 1950 to 2023, when SST data are most reliable. However, the analysis of ERSSTv5 from 1900 to 2023 also resulted in very similar ENSO and PAA modes and their associated PCs (Figure S6 in Supporting Information S1). In addition, the modes of ENSO and PAA based on ERSSTv5 over 1950–2023 are consistent with those in the independent data set HadISST over 1950–2022 (Figure S7 in Supporting Information S1).

The PAA mode may directly be associated with Atlantic Multidecadal Oscillation (AMO) (Kerr, 2000; Schlesinger & Ramankutty, 1994) in the Atlantic sector, which may further be associated with the Atlantic Meridional Overturning Circulation (AMOC; Delworth & Mann, 2000; Latif et al., 2006). The AMO mode may also contribute to the PAA in the Pacific sector in the form of the Pacific Decadal Oscillation (PDO; Tung et al., 2019; Werb & Rudnick, 2023; Zhang & Delworth, 2007). In the Arctic sector, the PAA is directly associated with the multidecadal fluctuation of the sea-ice area (Figure S8 in Supporting Information S1). Therefore, the PAA mode may represent a coupled atmosphere-ocean mode in the Norther Hemisphere as indicated by EOF1 of the SAT over the land and oceans in boreal summer at multidecadal timescale (Figure S9 in Supporting Information S1).

It should be noted that the quantification of MHWs may be dependent on defined thresholds such as the SST climatology over 1982–2011 in this study (Amaya et al., 2023) and the SST percentile above the climatological SSTs (Huang, Wang, et al., 2021). The super-MHWs represent extreme MHWs (Sen Gupta et al., 2020) above the maximum SST, but the maximum SST may also be dependent on the time period, which is quantified over 1982–2022 in this study. However, overall results were consistent as indicated in Huang, Wang, et al. (2021).

We note that the warming trend in this study is considered linear (Wang et al., 2022). One may argue that the linear warming trend may be subjective and could be non-linear (Deser & Phillips, 2021; Frankignoul et al., 2017; Xu et al., 2022). Further analyses (see details in Supporting Information S1) indicate that, when a quadratic warming trend at centennial timescale starting from 1900 is applied and filtered out from the SSTAs, the low-frequency mode remains unaffected (Figure S10 in Supporting Information S1). However, when a quadratic warming trend at decadal timescale starting from 1950 is applied and filtered out from the SSTAs, the low-frequency mode is damped greatly after 2000, which is demonstrated in the averaged SSTA in the North Atlantic (Figure S11 in Supporting Information S1). Therefore, caution should be taken when applying a non-linear trend.

In conclusion, the results shown in this study are consistent across different data sets and for analyses over different time periods. The SSTs in 2023 were record high across regions of the global oceans; and the record-high SSTs resulted from a combination of warming trend, PAA, and ENSO.

Data Availability Statement

Data sets used in this study are openly available: ERSSTv5 (Huang et al., 2017b), CMC SST (CMC, 2016), OSTIA SST (UKMO, 2012), ERA5 SAT (Hersbach et al., 2023), DOISST v2.1 (Huang, Liu, et al., 2021) at https://www.ncei.noaa.gov/data/sea-surface-temperature-optimum-interpolation/v2.1, HadISST (Rayner et al., 2003) at https://www.metoffice.gov.uk/hadobs/hadisst, and NCEP ice concentration (Grumbine, 2014) at https://ftp.ncep.noaa.gov/data/nccf/com/seaice_analysis/prod.

Acknowledgments
Authors thank two anonymous reviewers for their precious comments on this study. JAC and LC were supported by the NOAA Climate Program Office (NA20OAR4310339).

References

Amaya, D., Jacox, M. G., Fewings, M. R., Saba, V. S., Stuecker, M. F., Rykaczewski, R. R., et al. (2023). Marine heatwaves need clear definitions so coastal communities can adapt. *Nature*, *616*(7955), 29–32. https://doi.org/10.1038/d41586-023-00924-2

Brasnett, B., & Colan, D. S. (2016). Assimilating retrievals of sea surface temperature from VIIRS and AMSR2. *Journal of Atmospheric and Oceanic Technology*, *33*(2), 361–375. https://doi.org/10.1175/JTECH-D-15-0093.1

Canada Meteorological Center. (2016). GHRSST Level 4 CMC 0.1 deg global sea surface temperature analysis [Dataset]. *Ver. 3.0. PO.DAAC, CA, USA*. https://doi.org/10.5067/GHCMC-4FM03

Delworth, T. L., & Mann, M. E. (2000). Observed and simulated multidecadal variability in the Northern Hemisphere. *Climate Dynamics*, *16*(9), 661–676. https://doi.org/10.1007/s003820000075

Deser, C., & Phillips, A. S. (2021). Defining the internal component of Atlantic Multidecadal Variability in a changing climate. *Geophysical Research Letters*, *48*(22), e2021GL095023. https://doi.org/10.1029/2021GL095023

Donlon, C. J., Martin, M., Stark, J., Roberts-Jones, J., Fiedler, E., & Wimmer, W. (2012). The Operational Sea Surface Temperature and sea Ice Analysis (OSTIA) system. *Remote Sensing of Environment*, *116*, 140–158. https://doi.org/10.1016/j.rse.2010.10.017

Frankignoul, C., Gastineau, G., & Kwon, Y. O. (2017). Estimation of the SST response to anthropogenic and external forcing and its impact on the Atlantic multidecadal oscillation and the Pacific decadal oscillation. *Journal of Climate*, *30*(24), 9871–9895. https://doi.org/10.1175/jcli-d-17-0009.1

Grumbine, R. W. (2014). Automated sea ice concentration analysis history at NCEP 1996–2012. Marine Modeling and Analysis Branch. *Tech. Note*, *321*, 39.

Hersbach, H., Bell, B., Berrisford, P., Biavati, G., Horányi, A., Muñoz Sabater, J., et al. (2023). ERA5 monthly averaged data on single levels from 1940 to present [Dataset]. *Copernicus Climate Change Service (C3S) Climate Data Store (CDS)*. https://doi.org/10.24381/cds.f17050d7

Hersbach, H., Bell, B., Berrisford, P., Hirahara, S., Horányi, A., Muñoz-Sabater, J., et al. (2020). The ERA5 global reanalysis. *Quart. J. Roy. Meteor. Soc.*, *146*(730), 1999–2049. https://doi.org/10.1002/qj.3803

Hobday, A. J., Alexander, L. V., Perkins, S. E., Smale, D. A., Straub, S. C., Oliver, E. C., et al. (2016). A hierarchical approach to defining marine heatwaves. *Progress in Oceanography*, *141*, 227–238. https://doi.org/10.1016/j.pocean.2015.12.014

Holbrook, N. J., Scannell, H. A., Sen Gupta, A., Benthuysen, J. A., Feng, M., Oliver, E. C. J., et al. (2019). A global assessment of marine heatwaves and their drivers. *Nature Communications*, *10*(1), 2624. https://doi.org/10.1038/s41467-019-10206-z

Huang, B., L'Heureux, M., Hu, Z.-Z., & Zhang, H.-M. (2016). Ranking the strongest ENSO events while incorporating SST uncertainty. *Geophysical Research Letters*, *43*(17), 9165–9172. https://doi.org/10.1002/2016GL070888

Huang, B., Liu, C., Banzon, V., Freeman, E., Graham, G., Hankins, B., et al. (2021). Improvements of the Daily Optimum Interpolation Sea Surface Temperature (DOISST) version 2.1. *Journal of Climate*, *34*(8), 2923–2939. https://doi.org/10.1175/JCLI-D-20-0166.1

Huang, B., Thorne, P. W., Banzon, V. F., Boyer, T., Chepurin, G., Lawrimore, J. H., et al. (2017a). Extended Reconstructed Sea Surface Temperature Version 5 (ERSSTv5), upgrades, validations, and intercomparisons. *Journal of Climate*, *30*(20), 8179–8205. https://doi.org/10.1175/JCLI-D-16-0836.1

Huang, B., Thorne, P. W., Banzon, V. F., Boyer, T., Chepurin, G., Lawrimore, J. H., et al. (2017b). NOAA Extended Reconstructed Sea Surface Temperature (ERSST), version 5 [Dataset]. *NOAA National Centers for Environmental Information*. https://doi.org/10.7289/V5T72FNM

Huang, B., Wang, Z., Yin, X., Arguez, A., Graham, G., Liu, C., et al. (2021). Prolonged marine heatwaves in the Arctic: 1982–2020. *Geophysical Research Letters*, *48*(24), e2021GL095590. https://doi.org/10.1029/2021GL095590

Huang, B., Yin, X., Carton, J. A., Chen, L., Graham, G., Liu, C., et al. (2023). Understanding differences in Sea Surface temperature intercomparisons. *JTECH*, *40*(4), 455–473. https://doi.org/10.1175/JTECH-D-22-0081.1

Ignatov, A., Zhou, X., Petrenko, B., Liang, X., Kihai, Y., Dash, P., et al. (2016). AVHRR GAC SST reanalysis version 1 (RAN1). *Remote Sensing*, *8*(4), 315. https://doi.org/10.3390/rs8040315

Kerr, R. A. (2000). A North Atlantic climate pacemaker for the centuries. *Science*, *288*(5473), 1984–1985. https://doi.org/10.1126/science.288.5473.1984

Kuhlbrodt, T., Swaminathan, R., Ceppi, P., & Wilder, T. (2024). A Glimpse into the future: The 2023 ocean temperature and sea ice extremes in the context of longer-term climate change. *Bulletin America Meteorology Social*, *105*(3), E474–E485. https://doi.org/10.1175/BAMS-D-23-0209.1

Kutzbach, J. E. (1967). Empirical eigenvectors of sea-level pressure, surface temperature and precipitation complexes over North America. *Journal of Applied Meteorology*, *6*(5), 791–802. https://doi.org/10.1175/1520-0450(1967)006<0791:eeoslp>2.0.co;2

Latif, M., Collins, M., Pohlmann, H., & Keenlyside, M. (2006). A review of predictability studies of Atlantic sector climate on decadal time scales. *Journal of Climate*, *19*(23), 5971–5987. https://doi.org/10.1175/jcli3945.1

L'Heureux, M. L., Takahashi, K., Watkins, A. B., Barnston, A. G., Becker, E. J., Di Liberto, T. E., et al. (2017). Observing and predicting the 2015–16 El Nino. *Bulletin America Meteorology Social*, *98*(7), 1363–1382. https://doi.org/10.1175/BAMS-D-16-0009.1

Li, X., Hu, Z.-Z., McPhaden, M. J., Zhu, C., & Liu, Y. (2023). Triple-dip La Niñas in 1998–2001 and 2020–2023: Impact of mean state changes. *Journal of Geophysical Research*, *128*(17), e2023JD038843. https://doi.org/10.1029/2023JD038843

Oliver, E. C. J., Donat, M. G., Burrows, M. T., Moore, P. J., Smale, D. A., Alexander, L. V., et al., (2018). Longer and more frequent marine heatwaves over the past century. *Nature Communications*, *9*(1), 1324. https://doi.org/10.1038/s41467-018-03732-9

Parker, W. S. (2013). Ensemble modeling, uncertainty and robust predictions. *Wiley interdisciplinary reviews: Climate Change*, *4*(3), 213–223. https://doi.org/10.1002/wcc.220

Philander, S. G. (1989). El Niño, La Niña, and the Southern oscillation. *International Geophysics Series*, *46*(23), 2652–2662.

Rayner, N. A., Parker, D. E., Horton, E. B., Folland, C. K., Alexander, L. V., Rowell, D. P., et al. (2003). Global analyses of sea surface temperature, sea ice, and night marine air temperature since the late nineteenth century. *Journal of Geophysical Research*, *108*(D14), 4407. https://doi.org/10.1029/2002JD002670

Schlesinger, M. E., & Ramankutty, N. (1994). An oscillation in the global climate system of period 65–70 years. *Nature*, *367*(6465), 723–726. https://doi.org/10.1038/367723a0

Schmidt, G., Shindell, D., & Tsigaridis, K. (2014). Reconciling warming trends. *Nature Geoscience*, *7*(3), 158–160. https://doi.org/10.1038/ngeo2105

Schmidt, G. A. (2024). Climate models can't explain 2023's huge heat anomaly — We could be in uncharted territory. *Nature*, *627*(8004), 467. https://doi.org/10.1038/d41586-024-00816-z

Sen Gupta, A., Thomsen, M., Benthuysen, J. A., Hobday, A. J., Oliver, E., Alexander, L. V., et al. (2020). Drivers and impacts of the most extreme marine heatwaves events. *Scientific Reports*, *10*(1), 19359. https://doi.org/10.1038/s41598-020-75445-3

Titchner, H. A., & Rayner, N. A. (2014). The Met Office Hadley Centre sea ice and sea surface temperature data set, version 2: 1. Sea ice concentrations. *Journal of Geophysical Research: Atmospheres*, *119*(6), 2864–2889. https://doi.org/10.1002/2013JD020316

Tung, K. K., Chen, X., Zhou, J., & Li, K. F. (2019). Interdecadal variability in pan-Pacific and global SST, revisited. *Climate Dynamics*, *52*(3–4), 2145–2157. https://doi.org/10.1007/s00382-018-4240-1

UK Met Office. (2012). OSTIA L4 SST analysis (GDS2) [Dataset]. *Ver. 2.0. PO.DAAC, CA, USA*. https://doi.org/10.5067/GHOST-4FK02

Wang, S., Jing, Z., Sun, D., Shi, J., & Wu, L. (2022). A new model for isolating the marine heatwave changes under warming scenarios. *Journal of Atmospheric and Oceanic Technology*, *39*(9), 1353–1366. https://doi.org/10.1175/JTECH-D-21-0142.1

Werb, B. E., & Rudnick, D. L. (2023). Remarkable changes in the dominant modes of North Pacific sea surface temperature. *Geophysical Research Letters*, *50*(4), e2022GL101078. https://doi.org/10.1029/2022GL101078

Xu, T., Newman, M., Capotondi, A., Stevenson, S., DiLorenzo, E., & Alexander, M. (2022). An increase in marine heatwaves without significant changes in surface ocean temperature variability. *Nature Communications*, *13*(1), 7396. https://doi.org/10.1038/s41467-022-34934-x

Yang, C., Leonelli, F. E., Marullo, S., Artale, V., Beggs, H., Nardelli, B. B., et al. (2021). Sea surface temperature intercomparison in the framework of the copernicus climate change Service (C3S). *Journal of Climate*, *34*(13), 5257–5283. https://doi.org/10.1175/JCLI-D-20-0793.1

Zebiak, S. E., & Cane, M. A. (1987). A model El Niño–Southern oscillation. *Monthly Weather Review*, *115*(10), 2262–2278. https://doi.org/10.1175/1520-0493(1987)115,2262:AMENO.2.0.CO;2

Zhang, R., & Delworth, T. L. (2007). Impact of the Atlantic multidecadal oscillation on North Pacific climate variability. *Geophysical Research Letters*, *34*(23). https://doi.org/10.1029/2007gl031601